Journal of Luminescence 295 (2026) 121910

Contents lists available at ScienceDirect

Journal of Luminescence

journal homepage: www.elsevier.com/locate/jlumin

Full Length Article

Demonstrating polaron mediated photoluminescence in vanadates by a combined experimental and computational study

Jeffrey Zom [a,*], Alexandros Vasileiadis [b], Shuaishuai Yuan [c], Erik van der Kolk [a]

[a] Luminescence Materials, Delft University of Technology, Mekelweg 15, 2629 JB, Delft, The Netherlands
[b] Storage of Electrochemical Energy, Delft University of Technology, Mekelweg 15, 2629 JB, Delft, The Netherlands
[c] Department of Physics, McGill University, Sherbrooke Street West 845, QC H3A 0G4, Montréal, Canada

ARTICLE INFO

Keywords:
Vanadate
Luminescence
Charge-Transfer
Polaron
Self-trapped exciton

ABSTRACT

Photoluminescence in vanadate compounds has traditionally been attributed to charge-transfer transitions within isolated $[VO_4]^{3-}$ centres, with excitation and emission described using molecular orbitals. In previous work, we proposed an alternative mechanism: photoluminescence arises from conventional interband excitation, followed by electron polaron-mediated formation of self-trapped excitons. In this study, we provide further evidence for this model through spectroscopic measurements and ab initio calculations. Using density functional theory calculations on a series of alkali vanadates (MVO_3, M = Li, Na, K, Rb, Cs), we show that photoexcited electrons spontaneously localise on V^{5+} ions, leading to self-trapped exciton formation via hole localisation on neighbouring oxygen atoms. The calculated energies for band gaps and self-trapped excitons closely match experimental values obtained from diffuse reflectance and luminescence spectroscopy. Importantly, temperature- and time-resolved luminescence measurements reveal that quenching predominantly occurs before the formation of the luminescent state, challenging earlier models that assumed quenching to occur from the final emitting state. To explain this behaviour, we note that the width of the conduction band states is expected to govern the rate of electron trapping, and we indeed find a correlation between calculated bandwidths and measured quantum efficiencies. This suggests that non-radiative relaxation of free carriers at defects, prior to self-trapping, is the dominant quenching mechanism. Consequently, the electron self-trapping rate, the self-trapped exciton formation rate, and the defect concentration are expected to critically determine the luminescent efficiency of vanadate phosphors.

1. Introduction

The photoluminescence of phosphors based on vanadium oxide, so-called vanadates, is historically described as a charge-transfer transition, whereby the electronic states involved in the luminescent process originate in molecular orbital theory [1]. In short, the V^{5+} cations surrounded by four O^{2-} anions within the crystal structures are treated as isolated $[VO_4]^{3-}$ groups responsible for the absorption and emission of ultraviolet and visible light, respectively. Excitation is viewed as a charge-transfer transition, in which the electron density of the four oxygen ligands is equivalently transferred to their central vanadium ion, which effectively gains an electron and changes to the V^{4+} oxidation state. The formed excited state then relaxes by a change in total electronic spin (singlet to triplet state). Emission can be thought of as the reverse process of excitation with the addition of a change in total electronic spin (triplet to singlet state).

In our previous work [2], we criticised this mechanism on the basis of multiple inconsistencies between what would be theoretically expected and is observed. In short, on the basis of the aforementioned mechanism, one would expect the excitation spectra to be narrow (relative to those of interband transitions), the energy of the emission to be correlated to that of excitation, and emission from the triplet states, as well as excitation to the singlet states, to be possible (although relatively weak). In contrast, the excitation spectra of vanadates appear to be complex and broad (emission after up to 10 eV photoexcitation has been demonstrated [3]), the energy of the emission is uncorrelated to that of excitation, and both excitation to the triplet and emission from the singlet states are never observed.

In light of these observations, as well as prior experimental and theoretical studies demonstrating the delayed formation of V^{4+} after photoexcitation [4], we propose an alternative mechanism underlying the luminescent properties of vanadates. Specifically, we suggest that the

* Corresponding author.
E-mail address: j.zom@tudelft.nl (J. Zom).

https://doi.org/10.1016/j.jlumin.2026.121910
Received 13 January 2026; Received in revised form 13 March 2026; Accepted 7 April 2026
Available online 14 April 2026

excitation is more accurately described as a conventional interband transition, while the emission results from self-trapped excitons formed following initial electron polaron formation.

In this work, we present strong evidence supporting our proposed mechanism and discuss its significance in understanding the origin of quenching in vanadates. We selected the series of alkali metavanadates (MVO_3, M = Li, Na, K, Rb, Cs) for investigation, since there appears to be a general trend in which the luminescence efficiency of vanadate complexes containing alkali metals increases by several orders of magnitude from Li to Cs [2], the origin of which is not yet understood. Additionally, the extensive existing literature on these compounds provides valuable support for interpreting our experimental results. We first present the measured time- and temperature-dependent luminescence properties. We then demonstrate how DFT + U calculations on the same compounds concerning their electronic structure provide novel insights into these experimental results.

2. Methods

2.1. Alkali metavanadate synthesis

Alkali metavanadate (MVO_3, M = Li, Na, K, Rb, Cs) powders were synthesized by conventional solid-state reaction. Alkali carbonates (Li_2CO_3, 99.997 %, Merck; Na_2CO_3, 99.95 %, Merck; K_2CO_3, 99.997 %, Alfa Aesar; Rb_2CO_3, 99.8 %, Merck; Cs_2CO_3, 99.9 %, Merck) were mixed in stoichiometric ratios with 500 mg of vanadium(V) oxide (V_2O_5, 99.9 %, Merck) and ground with a granite mortar and pestle for approximately 20 min. The mixtures were heated in alumina crucibles in a tube furnace (Nabertherm RHTH 120-600/18) at 450 °C for 12 h. Grinding and annealing were repeated twice to ensure complete reaction and to obtain phase-pure MVO_3, as confirmed by X-ray diffraction (see Figure S1). The resulting white powders were stored in sealed containers under ambient conditions.

2.2. Experimental techniques

Bragg-Brentano X-ray diffraction (Malvern Panalytical X 'Pert3 MRD) measurements were performed on all samples at room temperature using Cu Kα radiation at λ = 1.5406 Å, scanning from 5° to 50° (2θ) over a period of 50 minutes. Temperature and excitation wavelength-dependent emission spectra were measured using a custom setup equipped with a Xenon arc lamp (Newport 66921), a double monochromator (Gemini 180), a photodiode (Opto Diode UVG100) and an electrometer (Keithley 6517A) to correct for the wavelength-dependence of the lamp intensity (as well as its fluctuations over time), a helium cryostat (Janis CCS-100/204) with a heater controlled using a temperature controller (Lakeshore 331), and a spectrometer (Ocean View QE-Pro). For the temperature-dependent time-resolved measurements, the same cryostat and temperature controller were used, with the addition of a laser (EKSPLA NT230) at 350 nm with a pulse-length of ca. 10 ns and a pulse-frequency of 25 Hz, a double monochromator (Acton SP2300) and a photomultiplier tube (Philips XP2020Q) that was connected to a digitiser (CAEN DT5724F). For emission spectra and decay measurements, a 385 nm (Newport 10CGA) long-pass filter was placed between the sample and the detector, while a 430 nm (Semrock FF01) long-pass filter was used for measuring excitation spectra. All emission spectra were corrected for the wavelength-dependent transmission of the applied long-pass filter, and for the wavelength-dependence of the spectrometer.

2.3. First-principles calculations

All calculations were performed with the Vienna Ab Initio Simulation Package (VASP) [5–9]. The generalised gradient approximation (GGA) with the Perdew-Burke-Ernzerhof (PBE) functional was used [10]. The strong on-site Coulomb interactions of localised electrons are often poorly described by GGA [11–14]. Therefore, an on-site Coulomb interaction of 3.25 eV, an effective Hubbard U parameter described by Dudarev et al. [15], was added to the 3d electrons of vanadium. This is the U value calculated for vanadium in the Materials Project, which was obtained by fitting the U-dependent calculated binary formation enthalpies of vanadium oxides with different oxidation states to experimental values, described in the work of Wang et al. [16]. Note that earlier research has shown that use of the PBE functional as well as the application of a U parameter (3 eV) lead to a significant improvement in the calculated band gap and lattice parameters for various vanadium oxides [17]. Projector augmented wave (PAW) potentials were used in the form: Li ($1s^2 2s^1$), Na ($2s^2 2p^6 3s^1$), K ($3s^2 3p^6 4s^1$), Rb ($4s^2 4p^6 5s^1$), Cs ($5s^2 5p^6 6s^1$), V ($3s^2 3p^6 4s^2 3d^3$), O ($2s^2 2p^4$). The initial atomic configurations of $LiVO_3$ and $NaVO_3$ (space group C2/c) and KVO_3, $RbVO_3$, and $CsVO_3$ (space group Pbcm) were obtained from the Materials Project [18]. Energy cut-offs for plane waves of 520 eV were used. When the energy difference between two calculations was less than 1×10^{-6} eV, the electronic configuration was considered converged. When all interatomic Hellmann-Feynman forces were below 1×10^{-2} eV Å^{-1}, the atomic configuration was considered to be converged. All calculations were performed with spin polarisation. For geometry relaxation of the unit cells, the cell size and shape were allowed to vary. For calculations concerning polarons, $1 \times 1 \times 2$ and $2 \times 2 \times 1$ supercells, constructed using relaxed unit cells, were used for crystals with, respectively, the space group C2/c and Pbcm, and the size and shape of the cells were fixed. Γ-centred k-point grids with a comparable uniform sampling density were used: $4 \times 4 \times 8$ and $8 \times 8 \times 4$ for unit cells with, respectively, the space group C2/c and Pbcm, and $4 \times 4 \times 4$ for supercells. For calculations involving electron polarons, an additional electron was added to the supercell with a uniform compensating positive background charge. To achieve a stable polaron solution, one often needs to gently break the symmetry of the pristine lattice. Therefore, for geometry relaxation calculations concerning electron polarons, the symmetry of the supercell lattice was broken by locally distorting one vanadium site by elongating the V-O bonds to its four neighbouring oxygen atoms by 0.1 Å. For the calculation of the self-trapped exciton triplet state, similar to earlier works [19,20], the ΔSelf-Consistent Field (ΔSCF) method was employed. This approach enables the description of specific excited-state configurations within the framework of ground-state density functional theory (DFT) by enforcing a constrained occupation of the Kohn-Sham states. In practice, the electronic configuration corresponding to the STE was obtained by constraining the spin state to a triplet configuration (ΔS = 1), implemented by restricting the total magnetic moment to $2\mu_B$. Geometry relaxation was performed using the previously optimized electron polaron structure as the starting configuration. The ΔSCF procedure allows variational optimization of the total energy under the imposed occupation constraints, yielding a self-consistent excited-state solution that reflects the localized nature of the STE. In accordance with the Franck-Condon principle, the vertical emission energy was determined as the total energy difference between the constrained triplet state and the singlet ground state at identical atomic coordinates.

3. Results & discussion

3.1. Experimental study

3.1.1. Absorption & excitation

In order to obtain information on the wavelength-dependence of the absorption of the alkali vanadates, diffuse reflectance measurements were performed. To quantify the absorption, on the basis of Kubelka–Munk theory [21], the measured reflectance was converted into the remission function. The absorption across the series of compositions, shown in Fig. 1, is strikingly similar. All vanadates have an absorption onset at ca. 3.1 eV with similar features at higher energy, namely peaks in absorption at ca. 3.5 eV and 4.3 eV and an increase in absorption from 5.0 eV to higher energy. These features in the absorption appear to be

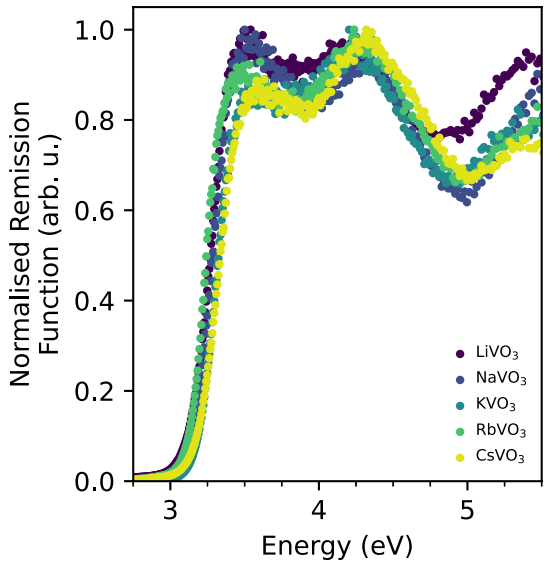

Fig. 1. The normalised remission function, representing the absorption strength, as a function of energy for all alkali metavanadates. The data were calculated using the Kubelka–Munk equation applied to diffuse reflectance spectra measured at room temperature.

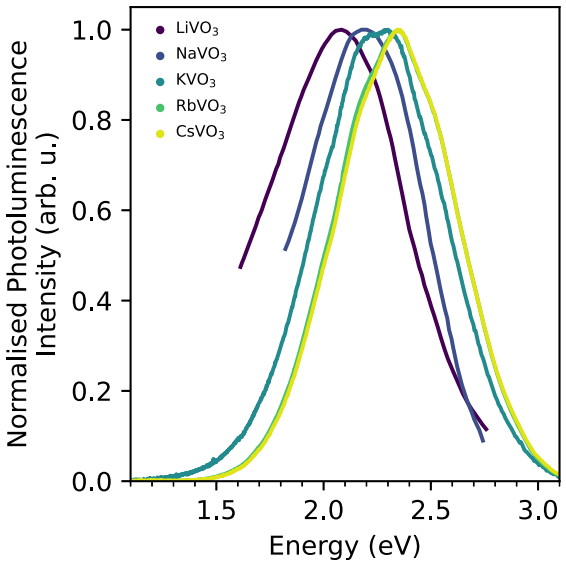

Fig. 3. The normalised emission spectra of all alkali metavanadates. The spectra of KVO_3, $RbVO_3$, and $CsVO_3$ were measured at room temperature, the spectra of $LiVO_3$ and $NaVO_3$ were obtained from Berdnikov and Zelikin and were measured at 77 K [25].

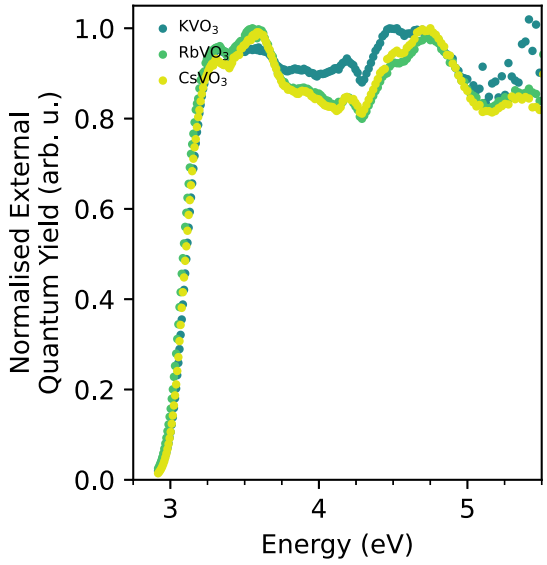

Fig. 2. The normalised external quantum yield as a function of energy, i.e. the excitation spectra, for the alkali metavanadates KVO_3, $RbVO_3$, and $CsVO_3$, at room temperature. No luminescence was measured for $LiVO_3$ and $NaVO_3$. Emission intensities were calculated by integrating over the entire emission spectra.

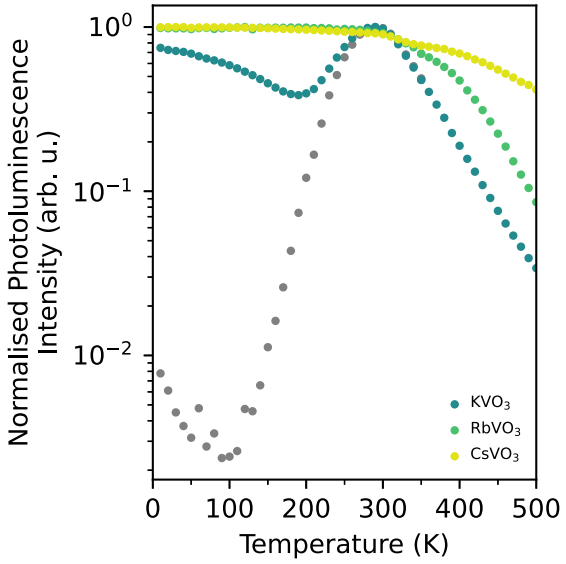

Fig. 4. Normalised photoluminescence intensity as a function of temperature of KVO_3, $RbVO_3$, and $CsVO_3$, measured between 10 K and 500 K. The emission intensities were obtained by integrating over the entire emission spectra. The gray data points represent the calculated temperature-dependent intensities of the high-energy emission band of KVO_3 based on Gaussian deconvolution.

an inherent property shared across this series of vanadates, given that such features were not observed in oxides with similar absorption onsets, excluding the possibility of an apparent structure caused by an instrumental response (see Figure S2).

The excitation spectra for KVO_3, $RbVO_3$, and $CsVO_3$ (of which the corresponding emission will be discussed later), shown in Fig. 2, further support this claim as they share similar features. For $LiVO_3$ and $NaVO_3$ no luminescence was observed, even when cooled to 10 K, so that no excitation spectra could be measured. As the absorption spectra are similar to the excitation spectra, we can conclude that the internal quantum efficiency appears to be roughly constant for this energy range.

3.1.2. *Temperature-dependent Emission*

At room temperature, the photoluminescence of KVO_3 was (weakly) observable by eye, while that of $RbVO_3$ and $CsVO_3$ appeared bright. Their luminescence at room temperature is shown in Fig. 3. The photoluminescence reported by Berdnikov and Zelikin for $LiVO_3$ and $NaVO_3$ measured at 77 K (since no luminescence was reported at room temperature) was added to this figure for comparison across the series. From $LiVO_3$ to $CsVO_3$ the emission spectrum shifts towards lower wavelengths. In line with earlier reports [22], the measured luminescence intensity increases in the series from $LiVO_3$ to $CsVO_3$. It should be noted that many earlier studies mentioned that they were also unable to measure the photoluminescence of $LiVO_3$ and $NaVO_3$ [22–24]. It appears that the synthetic method used by Berdnikov and Zelikin [25], which differs from the conventional solid-state method by using a solution-based method, is crucial to obtain photoluminescence in $LiVO_3$ and $NaVO_3$. Based on this observation, we infer that, in comparison to the other vanadates, these compounds are either much more susceptible to the

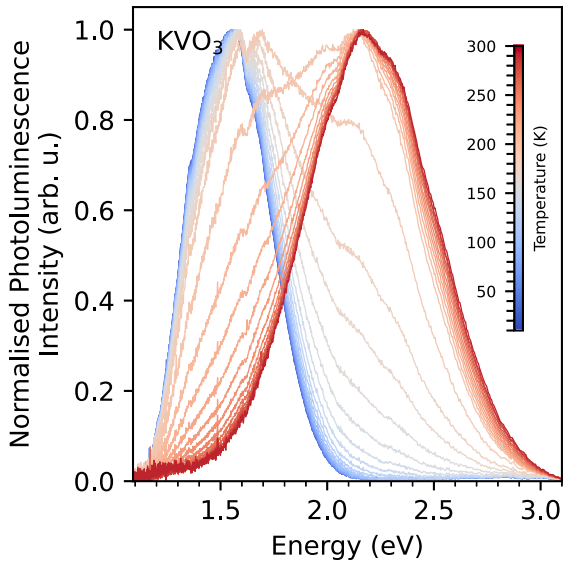

Fig. 5. Normalised emission spectrum of KVO_3 as a function of temperature measured between 10 K (blue) and 500 K (red). The excitation wavelength was 350 nm.

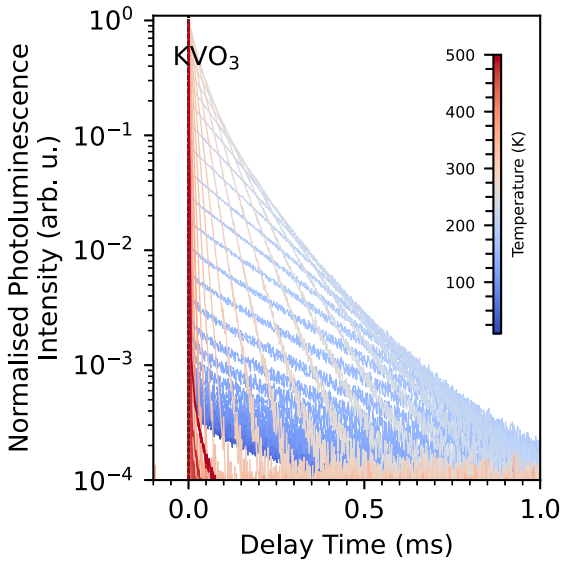

Fig. 7. Luminescence intensity as a function of delay time of KVO_3 measured between 10 K (blue) and 300 K (red). The excitation and emission wavelengths were respectively 350 nm and 550 nm.

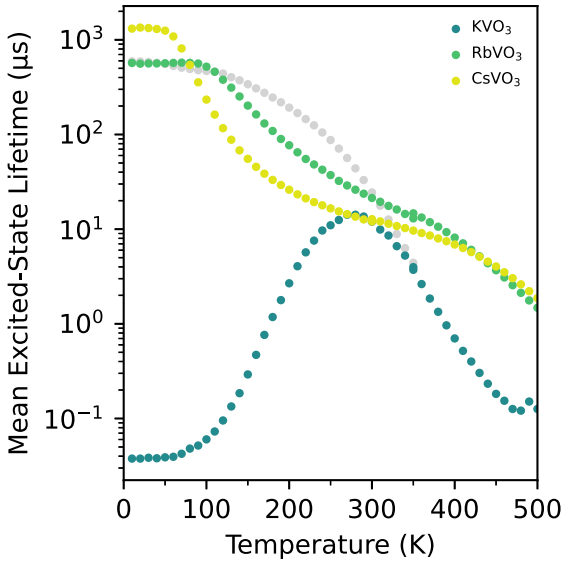

Fig. 6. Mean excited-state lifetime as a function of temperature between 10 K and 500 K of KVO_3, $RbVO_3$, and $CsVO_3$, calculated using Equation 1. Gray data points represent the temperature-dependent lifetime of the slow decay component in KVO_3, extracted from integration over the tail region of the decay curve. The excitation and emission wavelengths were 350 nm and 550 nm, respectively.

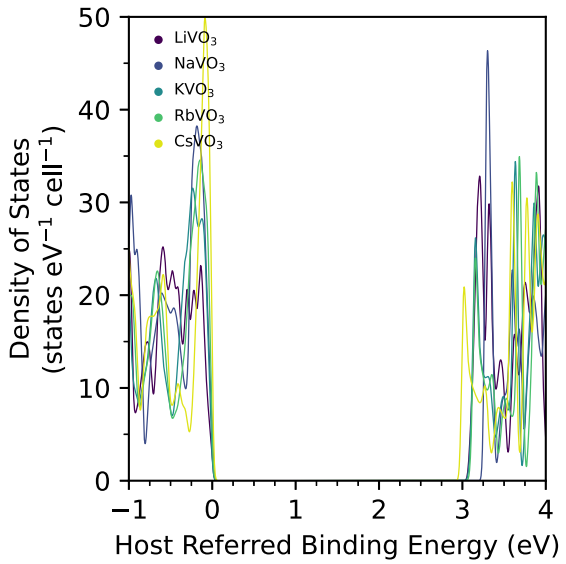

Fig. 8. Calculated DOS as a function of energy, with respect to the valence band edge, calculated for all alkali metavanadates. For fair comparison, the DOS of $NaVO_3$ and $LiVO_3$ were scaled by a factor 0.5, as their unit cells contain twice the amount of atoms (due to their lower symmetry) compared to the other vanadates.

creation of defects during synthesis and/or suffer more drastically in their quantum efficiency from defects.

The intensity of the photoluminescence of KVO_3, $RbVO_3$, and $CsVO_3$ was measured between 10 K and 500 K and is shown in Fig. 4. For KVO_3, the emission intensity initially decreases with increasing temperature, rises again from about 200 K, reaches a maximum near room temperature, and then decreases monotonically at higher temperatures. Interestingly, for KVO_3, the emission spectrum changes significantly with temperature; see Fig. 5. This stands in contrast to the emission spectra measured for $RbVO_3$ and $CsVO_3$, which only experience a small blueshift as the temperature increases (see Figure S3). At 10 K, the emission spectrum of KVO_3 shows a broad band centred at approximately 1.7 eV, composed of a vibronic progression, while at 300 K it appears as a single broad band centred at about 2.2 eV. As the temperature increases from ca. 150 K to 250 K, the lower-energy band decreases in intensity while the higher-energy band increases in intensity. The temperature-dependent intensity of these individual bands is also shown in Fig. 4. One earlier study on KVO_3 also reported the presence of a lower energy band at a low temperature [24], while two other studies did not measure a similar temperature dependence of the high-energy band [22,25]. Given these conflicting reports on the presence of the lower-energy emission band, it cannot be an intrinsic property of KVO_3 and we instead attribute its origin to the presence of a phase contamination or defects, which are commonly, but not necessarily, created in the synthesis of KVO_3. Because the excitation spectra of the low- and high-energy bands appeared identical, we believe that defect-related luminescence is more likely. In contrast to the emission of $RbVO_3$ and $CsVO_3$, the intrinsic emission of KVO_3 appears to be thermally activated, while the onset of

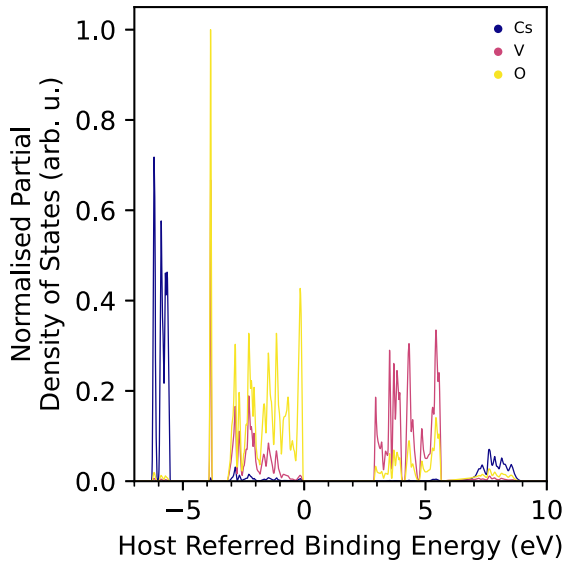

Fig. 9. Calculated normalised partial DOS as a function of energy, with respect to the valence band edge, calculated for Cs, V, and O in $CsVO_3$.

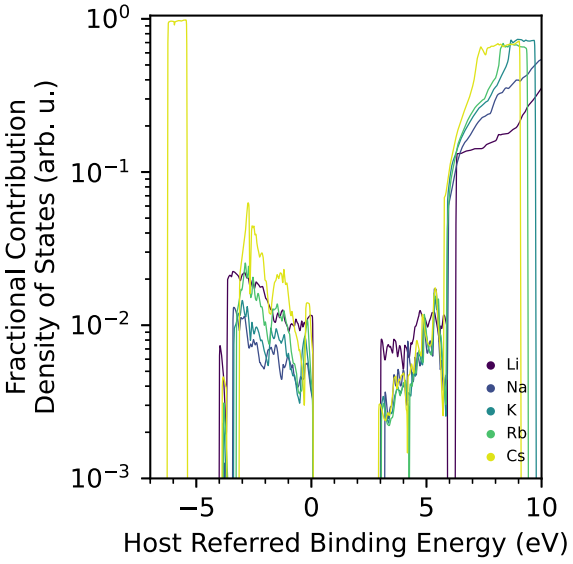

Fig. 10. Calculated fractional contribution of the alkali metal to the total DOS as a function of energy, with respect to the valence band edge, for all alkali metavanadates.

their thermal quenching occurs around the same temperature, roughly at room temperature.

3.1.3. Time-resolved emission

The time-resolved emission of KVO_3, $RbVO_3$, and $CsVO_3$ following a laser pulse was measured between 10 K and 500 K. Fig. 6 shows the temperature-dependent average excited-state lifetime of the emission of KVO_3, $RbVO_3$, and $CsVO_3$ calculated based on Eq. (1):

$$\langle \tau \rangle = \int_0^\infty I_{PL}(t)/I_{PL}(0)dt \quad (1)$$

where $I_{PL}(t)$ denotes the average measured intensity of photoluminescence at time t after a laser pulse at t = 0 [26]. The temperature-dependent decays of $RbVO_3$ and $CsVO_3$ are considerably simpler than that of KVO_3, so we will first discuss these to facilitate the interpretation of the behaviour of KVO_3.

Both $RbVO_3$ and $CsVO_3$ show mono-exponential decay at all temperatures (see Figure S4 and S5), of which the concomitant excited-state lifetime decreases strongly with increasing temperature. Considering that the intensity of the luminescence does not change for $RbVO_3$ and $CsVO_3$ up to ca. 300 K, the orders-of-magnitude decrease in their lifetime in this range, respectively, from 570 μs to 21 μs and 1350 μs to 15 μs, indicates a strongly temperature-dependent radiative decay rate. Above this temperature, $RbVO_3$ and $CsVO_3$ start to quench (see Fig. 4), further reducing their excited-state lifetime, predominantly by an increase in their non-radiative decay rate. A possible explanation for the strong temperature dependence of their radiative decay rates is that there are multiple excited states with different radiative decay rates that are thermally coupled. This could also explain the slight blueshift observed in their luminescence with increasing temperature. A thermally coupled excited-state model is indeed able to describe the temperature dependence of the excited-state lifetime of $RbVO_3$ and $CsVO_3$ very well up to ca. 300 K, above which thermal quenching causes deviation (see Figure S5).

The decay of KVO_3 (see Fig. 7) is multi-exponential at all temperatures and appears to consist of two mono-exponential components; one with a comparatively short lifetime (below 0.1 μs at 10 K), and one with a comparatively long lifetime (ca. 600 μs at 10 K) of which the lifetime decreases strongly with increasing temperature. The amplitude of the long-lifetime component relative to that of the short-lifetime component is comparatively low at 10 K, but increases with increasing temperature, most significantly from ca. 150 K, so that the short-lifetime component is essentially zero above 250 K. We interpret the complex temperature dependence of KVO_3 as follows. The previously attributed defect-related emission at low temperatures has a short decay time, whereas intrinsic KVO_3 luminescence has a relatively long decay time. This interpretation is supported by the fact that at room temperature, the lifetime of vanadates is expected to be on the order of several microseconds [2], which often significantly increases at lower temperatures [27], as we have also observed for $RbVO_3$ and $CsVO_3$. At low temperatures, even though the luminescence was measured at 550 nm, mainly the defect-related luminescence is measured because of its comparatively high intensity and broad character. As the temperature increases, the intensity of intrinsic KVO_3 luminescence increases, thereby increasing the relative component of the long-lifetime decay between 150 K and 250 K, the same range in which the relative intensity between the bands changes.

3.2. Computational study

In order to obtain deeper insights into the origin of the experimentally obtained results, we have performed spin-polarised DFT + U calculations on the same alkali vanadates. Our results support a mechanism in which luminescence in vanadates originates from (1) interband excitation generating free charge carriers, (2) barrierless localisation of electrons on individual vanadium ions (electron polaron formation), and (3) subsequent hole localisation induced by these electron polarons, leading to self-trapped exciton formation.

3.2.1. Band Structure & band gap

Fig. 8 shows the calculated density of states (DOS) of the alkali vanadates. According to these calculations, all band gaps have a size of ca. 3 eV. These band gaps are in good agreement with the onset of absorption shown in Fig. 1 and with the onset of the excitation spectrum shown in Fig. 2. Fig. 9 illustrates, using $CsVO_3$ as an example, that the valence and conduction bands in alkali metavanadates are predominantly characterised by contributions from respectively the oxygen and vanadium atoms. In contrast, the alkali metals have a negligible contribution to the DOS of the valence and conduction band, illustrated in Fig. 10 for all alkali metavanadates.

Fig. 11A and Fig. 11B respectively show the concomitant electronic band structures along high symmetry points in the Brillouin zone of the alkali vanadates with space group C2/c ($LiVO_3$ and $NaVO_3$) and of the alkali vanadates with space group Pbcm (KVO_3, $RbVO_3$, and $CsVO_3$). Interestingly, all calculated band gaps are indirect, while their direct

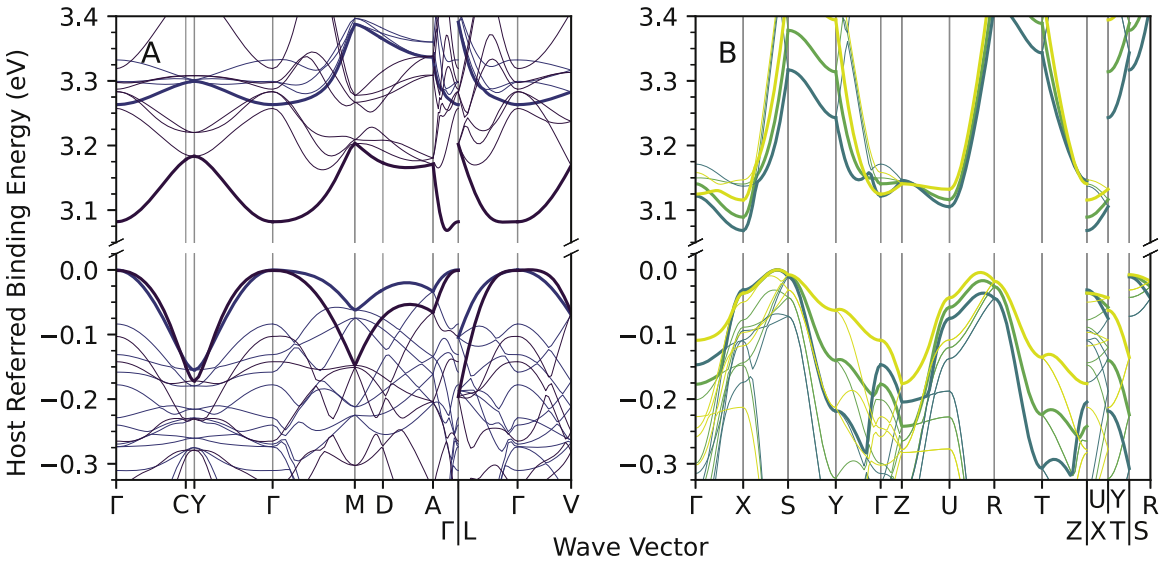

Fig. 11. Calculated energy, with respect to the valence band edge, as a function of wave vector along a high symmetry path. Figure A shows those calculated for $LiVO_3$ and $NaVO_3$ (respectively purple and dark blue), Figure B shows those calculated for KVO_3, $RbVO_3$, and $CsVO_3$ (respectively blue, green, and yellow). The highest (lowest) band of those forming the valence (conduction) band are highlighted in bold. Relative reciprocal lengths were calculated between high symmetry points of $LiVO_3$ and KVO_3.

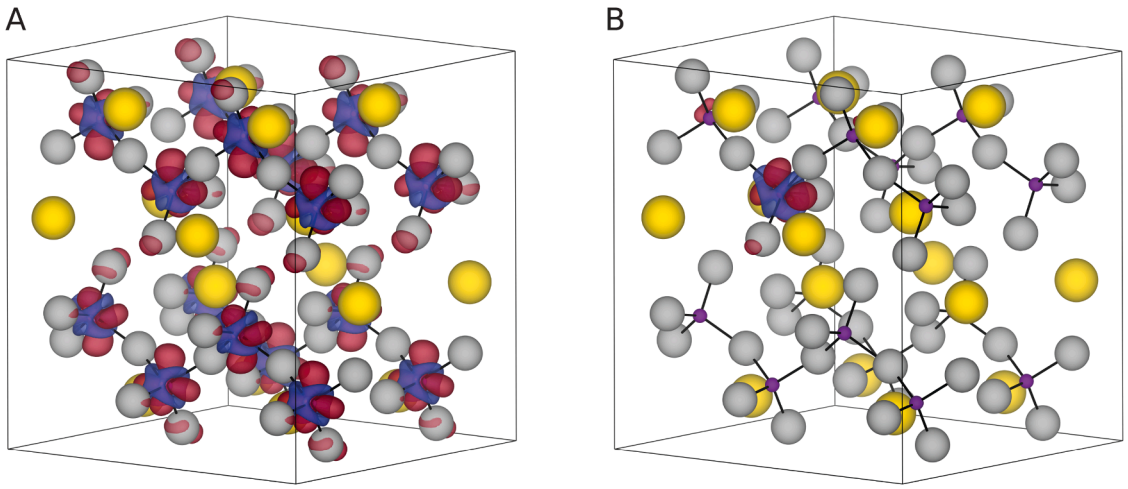

Fig. 12. Schematic representation of a supercell of $CsVO_3$ with an isosurface plot of the calculated electron density difference between the free electron and the ground state (A) and the electron polaron and the ground state (B). Positive and negative electron density differences are respectively coloured red and blue. Isosurface level values of $5 \times 10^{-4}\,e/a_0^3$ and $5 \times 10^{-3}\,e/a_0^3$ were used for Figure A and B respectively. Cs, V, and O atoms are respectively coloured yellow, purple and gray and shown with their ionic radii. Only the V-O bonds are shown in black. Figure was made using VESTA [50].

band gap is less than 100 meV larger. In such a case, their strength of absorption would not be limited by their indirect nature, while it would strongly prevent radiative recombination of free excitons. In agreement, we could find only one publication reporting the observation of free-exciton emission in a few vanadates [25]. A second notable trend is the narrowing of the electronic bands from the smaller to the larger cation within the same space group, along with a decrease in dispersion.

3.2.2. *Electron polaron formation*

We investigated the possibility of formation of electron polarons by adding an additional electron to the supercells, which occupies the lowest band in the conduction band. The additional electron in the conduction band is expected to be representative of an electron that is photoexcited (after hot carrier relaxation), apart from its missing interaction with an electron hole. We will discuss the involvement of the hole in the subsequent section.

Relaxation of both the electronic and ionic structures following the addition of an electron to the ground-state configuration results in minimal structural changes. The added electron remains delocalised over all vanadium atoms (see Fig. 12A), and the V-O bond lengths increase only slightly, by less than 0.01 Å. However, if we perturb the system before relaxation by increasing the V-O bond lengths around a single vanadium atom by a small amount (0.1 Å), we find that the relaxed electronic and ionic structures are significantly different; the additional electron has essentially become localised on the vanadium atom of the perturbed tetrahedron (see Fig. 12B), while its V-O bond lengths have changed significantly. In $CsVO_3$ for example, compared to the ground-state structure, the two V-O bonds part of the vanadate chain have expanded by ca. 0.12 Å while the other two V-O bonds have expanded by ca. 0.05 Å. A slight perturbation breaking the local symmetry of the system led to a lower-energy state, in which the initially delocalised free electron transformed into a localised electron polaron. It should be noted that the

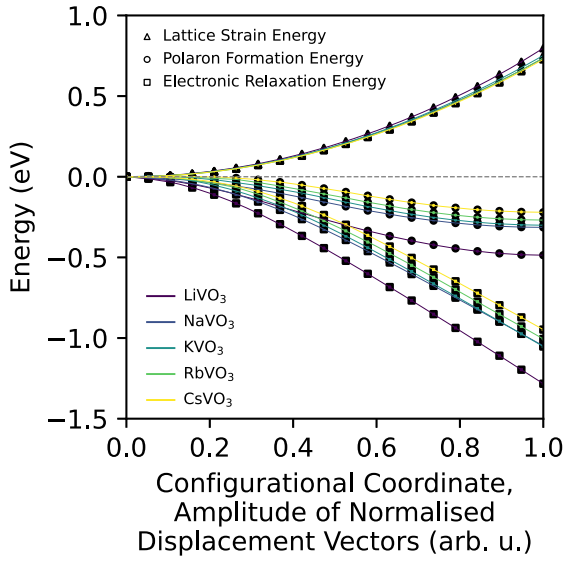

Fig. 13. Calculated lattice strain, polaron formation, and electronic relaxation energy, respectively indicated with triangular, circular, and square markers, as a function of the configurational coordinate for all alkali metavanadates indicated in colour. The configurational coordinates with values 0 and 1 refer to relaxed geometries of the unit cell with an additional electron obtained respectively without and with a perturbation of the initial geometry.

requirement of such a perturbation to identify the lower energy configuration does not imply the presence of an activation barrier in the process of electron polaron formation, as it is known that DFT calculations can fail to find the lowest-energy configuration [28].

Therefore, to obtain information on the activation energy required for polaron formation, we used a method based on the Mott-Stoneham picture [29], as described in detail by Yuan et al. [30]. In this approach, the separate contributions of lattice strain and electronic relaxation energy to the total energy are calculated as a function of the configurational coordinate along the relaxation path, see Eq. (2):

$$E_{tot}(Q) = E_{lat}(Q) + E_{el}(Q) \quad (2)$$

whereby E_{tot}, E_{lat}, and E_{el} are respectively the total energy, the lattice strain energy, and the electronic relaxation energy of the electron polaron, and Q is the configurational coordinate. Points within the configurational pathway between the initial and final configuration were calculated by adding a fraction of the calculated displacement vectors to the initial configuration.

Fig. 13 shows the calculated total energies of the alkali metavanadates as a function of the amplitude of the normalised displacement vectors. For all compounds, the energy is lower when the additional electron forms a localised electron polaron (amplitude = 1, corresponding to the final configuration) compared to when it remains delocalised (amplitude = 0, the initial configuration). The total energy of the polaronic state increases monotonically from $LiVO_3$ to $CsVO_3$, mirroring the trend observed in the emission band energies. We initially expected the lattice strain energy to decrease along the series from $LiVO_3$ to $CsVO_3$, due to the increasing polarizability of the alkali metal cations. This trend is indeed observed, but the effect is relatively minor. In contrast, the electronic relaxation changes significantly, being the main contributor to stabilising the polaron. Our calculations suggest that the total energy of the polaron is primarily determined by electronic relaxation, rather than lattice strain. Despite their minimal direct involvement in the electronic structure, the alkali cations still significantly influence the energetics of polaron formation through their impact on the host lattice environment.

The straightforward approach of using linear interpolation between the initial and final configurations may overestimate the activation barriers accompanying polaron formation, as it does not account for alternative (non-linear) pathways in the configurational space that could contain lower activation barriers. To obtain a more accurate estimate of the energy barrier, the nudged elastic band (NEB) method is typically used [31]. However, in our case, the results show that linear interpolation is sufficient, as no activation barrier for polaron formation was found in any of the compounds. The absence of an activation barrier suggests that any small deviation from the pristine configuration, which would be readily induced by vibrations, could cause self-trapping of (photoexcited) free electrons in these vanadates. Based on these results, it is therefore surprising that the luminescence of KVO_3 is thermally activated, and those of $LiVO_3$ and $NaVO_3$ are absent.

To understand the origin of the absence of an activation barrier in the formation of electron polarons in these compounds, we investigated the orbital projected band DOS. Because we have found that the results among the alkali metavanadates are qualitatively very similar, we will discuss the results in detail only for $CsVO_3$. We found that as the electron becomes trapped, an electronic state originating from the conduction band edge progressively lowers its energy, see Fig. 14A. We find that the band describing the state of the electron polaron is characterised mostly by the $3d_{z^2}$ and $3d_{x^2-y^2}$ orbitals of the vanadium atom that is part of the distorted tetrahedron, the same orbitals that describe the conduction band edge.

Calculations of the DOS along the same configurational coordinates concomitant with electron polaron formation, but without the addition of an additional electron, show only a marginal increase in the electronic energy of the bands constituting the valence band edge, see Fig. 14B. This thereby indicates that the increase in the electronic energy of these bands, depicted in Fig. 14A, is driven by the localisation of the additional electron, rather than the accompanying local deformation of the lattice. This gives a strong indication that electron polaron formation in vanadates is a requirement for, and thereby occurs prior to, localisation of the free hole (we will discuss the co-localisation of the hole in more depth in the next section).

Fig. 15 shows the contribution of the vanadium atom at the centre of the distortion to the total DOS as a function of the configurational coordinate. The data reveal that the additional electron becomes increasingly localised on the vanadium atom as relaxation proceeds. Interestingly, even in the fully relaxed configuration, a significant fraction of the electron density remains delocalised over the neighbouring oxygen atoms (0.26) and other vanadium atoms (0.10).

3.2.3. *Self-trapped exciton formation*

As we have discussed before, the electron polaron formation is accompanied by a significant increase in the energy of four bands at the VBE. These four bands are mainly associated with the electron density of the four oxygen atoms of the distorted vanadate group, i.e. surrounding the electron polaron. As a consequence of the presence of these raised bands, we hypothesise that the photoexcited delocalised free hole can relax, similar to the photoexcited electron, by localising on these oxygen atoms. Together with the electron polaron, the hole polaron would then form a so-called self-trapped exciton. In agreement, the sequential formation of electron polarons and STEs has been experimentally observed in $BiVO_4$ using transient absorption spectroscopy [4].

For all alkali metavanadates we have calculated the energy of the lowest triplet state, starting from their geometries of the relaxed electron polarons. During relaxation of the STE, the two V-O bonds in the vanadate group that are not part of the chain become further elongated, with the hole density primarily localised on the corresponding two oxygen atoms, see Fig. 16A. This is especially evident when comparing the electron density of the STE with that of the electron polaron, see Fig. 16B, which reveals that the key difference lies in the localisation of the hole on these two oxygen atoms.

The excited-state energies were calculated as the difference between the energies of the relaxed triplet states (the excited states) and the relaxed singlet states (the ground state) with the same configurational coordinates, as electronic relaxation occurs on a much smaller timescale

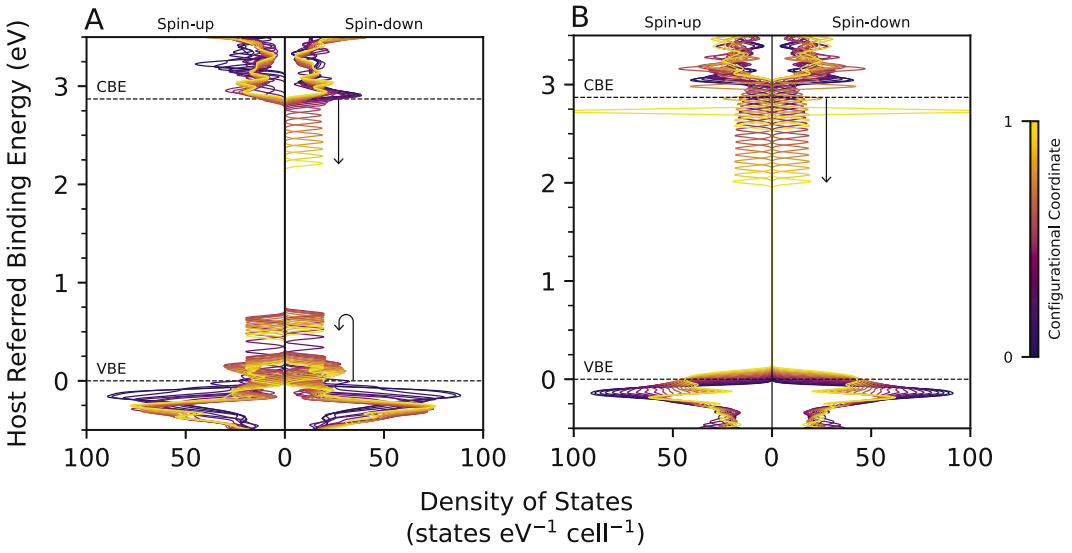

Fig. 14. Calculated spin decomposed DOS of $CsVO_3$ as a function of the configurational coordinate, indicated in colour, with (A) and without (B) the addition of an electron to the supercell, using the same atomic configurations. The configurational coordinates with values 0 and 1 refer to relaxed geometries of the unit cell with an additional electron obtained respectively without and with a perturbation of the initial geometry.

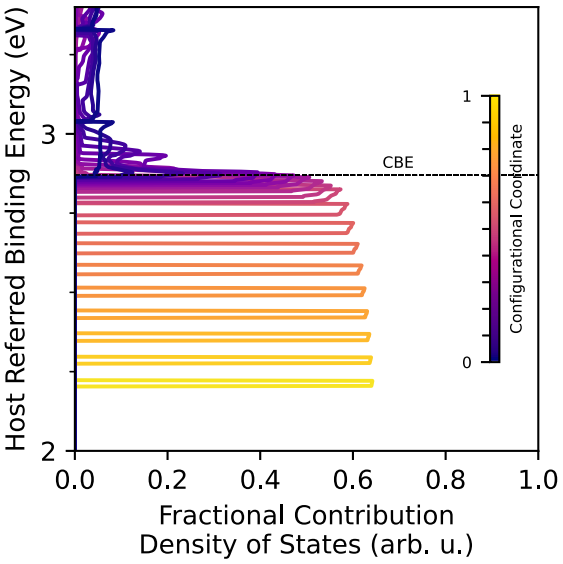

Fig. 15. Calculated contribution of the vanadium atom on which the electron becomes localised with respect to the total DOS, as a function of the configurational coordinate, indicated in colour.

than lattice relaxation (the Franck-Condon principle). Like the energy of the electron polaron, the calculated energy of the STE, the vertical emission energy, increases from $LiVO_3$ to $CsVO_3$, 1.89, 1.90, 1.93, 2.02, and 2.05 eV, following the experimentally observed trend in luminescence. The geometric means of the emission spectra were calculated to be 2.08, 2.19, 2.26, 2.33, and 2.34 eV, respectively. Despite the shortcomings of DFT regarding many-body interactions, the calculated energies of the STEs are in rough agreement with the peak emission energies, differing by only a few hundred meV.

Although the lowest-energy geometry of the fully relaxed STE differs significantly from the initial geometry of the electron polaron, the hole density is already fully localised in this initial configuration. Consequently, it was not possible to determine whether STE formation involves an activation barrier using the same approach applied for the electron polaron. This parameter could, however, play a crucial role: a nonzero activation barrier for STE formation that decreases from $LiVO_3$ to $CsVO_3$ can account for the temperature-dependent luminescence discussed earlier. A high activation barrier would prevent the system from reaching the luminescent excited state before nonradiative decay at any temperature, as observed for $LiVO_3$ and $NaVO_3$; a moderate barrier would allow luminescence only at elevated temperatures, as in KVO_3; and a low barrier would enable luminescence even at cryogenic temperatures, as observed for $RbVO_3$ and $CsVO_3$.

Identification of activation barriers associated with carrier self-trapping is commonly achieved using ultrafast transient absorption spectroscopy, which provides the temporal resolution necessary to follow lattice relaxation dynamics. Such measurements have shown that self-trapping can occur over a remarkably broad range of timescales, from several hundred picoseconds [32] to several picoseconds [33,34], down to the sub-picosecond regime [35,36]. A rapid onset generally indicates a barrierless or near-barrierless process, whereas delayed formation is consistent with the presence of an activation barrier that must be thermally overcome.

Notably, reports of self-trapped exciton luminescence are frequently associated with Cs-containing halides, including $Cs_2AgInCl_6$ [37,38], $CsCu_2I_3$ and $Cs_3Cu_2I_5$ [34], and Cs_2ZrCl_6 [36]. This apparent prevalence may partly reflect a research bias, as Cs-based compounds often crystallise in perovskite or perovskite-related structures that are extensively investigated for their optoelectronic properties, whereas materials containing smaller alkali cations more commonly adopt alternative structure types. [39]

It is worth noting that a reversed sequence of carrier localisation, where the hole localises prior to the electron, has been reported in many reports on self-trapped exciton formation in systems such as metal oxides [40], and alkali and alkaline-earth halides [41]. In contrast, we find no evidence supporting this mechanism in our calculations. When a hole was introduced by removing an electron from the system, no localisation of the hole density was observed upon structural relaxation. This remained the case both for relaxation starting from the pristine lattice and for relaxation starting from the lattice distortion associated with the electron polaron.

Nevertheless, we cannot fully exclude the possibility of hole trapping. Hole-polaron calculations are, similar to electron polaron calculations, subject to the well-known bias of density functional theory toward delocalised solutions due to self-interaction errors, and stabilising

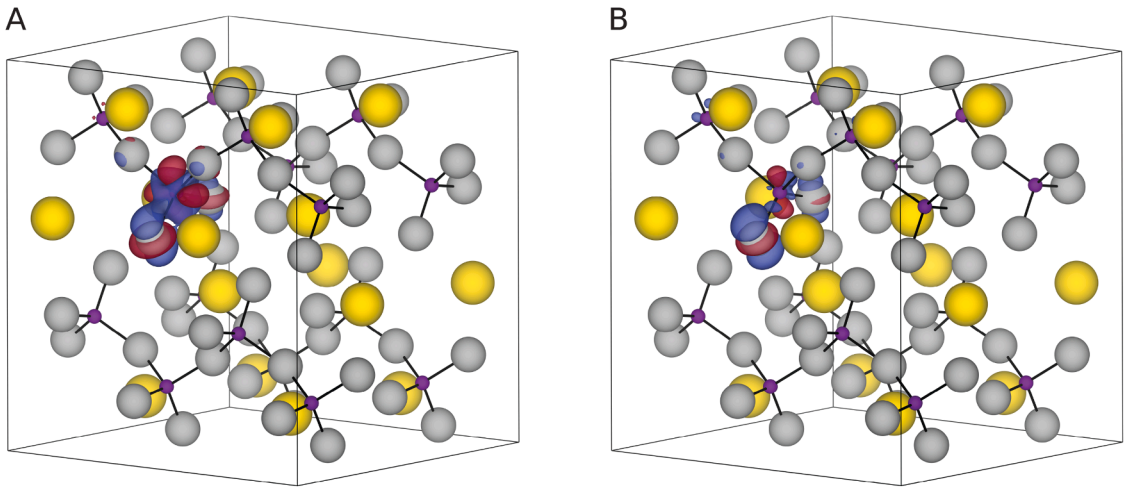

Fig. 16. Schematic representation of a supercell of $CsVO_3$ with an isosurface plot of the calculated electron density difference between the triplet state and the singlet state (A) and the triplet state and the electron polaron (B). Positive and negative electron density differences are respectively coloured red and blue. For both figures, an isosurface level value of 5×10^{-3} e/a_0^3 was used. Cs, V, and O atoms are respectively coloured yellow, purple and gray and shown with their ionic radii. Only the V-O bonds are shown in black. Figure was made using VESTA [50].

localised states may require corrective approaches such as the application of a Hubbard U potential [42]. While self-interaction errors affect both O 2p and V 3d states, the tendency toward artificial delocalisation is generally more pronounced for the latter due to their more localized nature, resulting in a larger self-interaction error [43].

4. Conclusions

We have performed a combined experimental and computational study on a series of alkali metavanadates (MVO_3, M = Li, Na, K, Rb, Cs) to gain insight into the general mechanism of photoluminescence of vanadates, as well as the origin of its quenching. The measured excitation and diffuse reflectance spectra show that absorption in these compounds occurs over a broad energy range from ca. 3 eV, which stands in contrast to the often reported narrow excitation bands interpreted to originate from localised charge-transfer transitions within the vanadate group ($[VO_4]^{3-}$). The presence of such broad absorption bands, as well as the close agreement between (DFT + U) calculated band gaps and onset of their absorption/excitation spectra, indicate that photoluminescence in vanadates is initiated by conventional interband transitions. We have further shown that barrierless relaxation of the photoexcited electron is possible through the formation of electron polarons localised on a single vanadium atom, and that their formation energy is mainly dictated by the degree of electronic relaxation rather than lattice strain. Electron polaron formation is accompanied by an increase in energy of several states originating from the valence band edge, characterised by 2p orbitals of the oxygen atoms surrounding the electron polaron. Calculations on the lowest energy triplet state show that the free hole can localise on these oxygen atoms, forming a self-trapped exciton (STE), further lowering the energy of the excited system. The calculated energies of these STEs follow the same trend as the energy of the observed emission bands and are, with a few hundred meV mismatch, in semi-quantitative agreement. The triplet character of the STEs was based on the experimentally observed long decay rate, on the order of 1 millisecond at 10 K. However, the measured temperature dependence of the luminescence intensities and excited-state lifetimes show that the radiative decay rates of these STEs are strongly temperature dependent, decreasing by several orders of magnitude from cryogenic temperatures to room temperature, suggesting the presence of multiple excited-state configurations with closely matched energies but strongly differing recombination rates. One possibility would be the presence of a higher energy singlet STE, which would explain both the experimentally observed blueshift in the luminescence band and the increase in radiative decay with increasing temperature.

While the origin of the stark contrast in luminescent efficiency among vanadate phosphors remains uncertain, our findings suggest a previously overlooked quenching pathway. Quenching has traditionally been assumed to occur from the luminescent excited state, yet our results indicate that it predominantly takes place before self-trapped exciton formation. Since the width of the conduction band states is expected to influence the rate of electron trapping, and given the observed correlation between calculated bandwidths and measured quantum efficiencies, we propose that non-radiative relaxation of free charge carriers at defects is the dominant quenching mechanism. Consequently, the electron self-trapping rate, the self-trapped exciton formation rate, and the defect concentration emerge as critical factors in determining the overall luminescent efficiency.

Further experimental work should utilise characterisation techniques which offer a high temporal resolution to probe the behaviour of free electrons and electron polarons in vanadates, such as transient absorption spectroscopy (TAS) [44,45], time-resolved microwave conductivity (TRMC) [46,47], and time-resolved angle-resolved photoemission spectroscopy (TR-ARPES) [48]. Further theoretical work should focus on determining the key factors influencing the rate of self-trapping of charge carriers in vanadates, for example through the use of time-dependent density functional theory (TDDFT) [49].

CRediT authorship contribution statement

Jeffrey Zom: Conceptualization, Methodology, Software, Validation, Formal analysis, Investigation, Data curation, Visualization, Writing – original draft, Writing – review & editing; **Alexandros Vasileiadis:** Conceptualization, Methodology, Resources, Writing – review & editing; **Shuaishuai Yuan:** Conceptualization, Methodology, Visualization, Writing – review & editing; **Erik van der Kolk:** Resources, Supervision, Project administration, Funding acquisition, Writing - review & editing.

Data availability

Data will be made available on request.

Funding

This work was supported by the Netherlands Organisation for Scientific Research (NWO) under project number ENPPS.TA.019.007.

Declaration of competing interest

The authors declare that they have no known competing financial interests or personal relationships that could have appeared to influence the work reported in this paper.

Supplementary material

Supplementary material associated with this article can be found in the online version at 10.1016/j.jlumin.2026.121910.

References

[1] G. Blasse, The luminescence of closed-shell transition-metal complexes. New developments, in: Luminescence and energy transfer. Structure and bonding, 42, Springer, Berlin, Heidelberg, 1980, pp. 1–41. https://doi.org/10.1007/3-540-10395-3_1

[2] J. Zom, E. Van der Kolk, Evaluation of the mechanism of luminescence and structure-efficiency relations of vanadate phosphors, J. Lumin. 286 (2025). article 121397. https://doi.org/10.1016/j.jlumin.2025.121397

[3] V.G. Zubkov, A.P. Tyutyunnik, N.V. Tarakina, I.F. Berger, L.L. Surat, B.V. Slobodin, G. Svensson, B. Forslund, B.V. Shul'gin, V.A. Pustovarov, A.V. Ishchenko, A.N. Cherepanov, Synthesis, crystal structure and luminescent properties of pyrovanadates $A_2CaV_2O_7$ (A = Rb, Cs), Solid State Sci. 11 (3) (2009) 726–732. https://doi.org/10.1016/j.solidstatesciences.2008.09.009

[4] J. Zhang, J. Shi, Y. Chen, K.H.L. Zhang, Y. Yang, Bimolecular self-trapped exciton formation in bismuth vanadate, J. Phys. Chem. Lett. 13 (42) (2022) 9815–9821. https://doi.org/10.1021/acs.jpclett.2c02596

[5] G. Kresse, J. Hafner, Ab initio molecular dynamics for liquid metals, Phys. Rev. B 47 (1) (1993) 558–561. https://doi.org/10.1103/physrevb.47.558

[6] G. Kresse, J. Furthmüller, Efficiency of ab-initio total energy calculations for metals and semiconductors using a plane-wave basis set, Comput. Mater. Sci. 6 (1) (1996) 15–50. https://doi.org/10.1016/0927-0256(96)00008-0

[7] G. Kresse, J. Furthmüller, Efficient iterative schemes for ab initio total-energy calculations using a plane-wave basis set, Phys. Rev. B 54 (16) (1996) 11169–11186. https://doi.org/10.1103/physrevb.54.11169

[8] G. Kresse, J. Hafner, Norm-conserving and ultrasoft pseudopotentials for first-row and transition elements, J. Phys. Condens. Matter 6 (40) (1994). article 8245. https://doi.org/10.1088/0953-8984/6/40/015

[9] G. Kresse, D. Joubert, From ultrasoft pseudopotentials to the projector augmented-wave method, Phys. Rev. B 59 (3) (1999) 1758–1775. https://doi.org/10.1103/PhysRevB.59.1758

[10] J.P. Perdew, K. Burke, M. Ernzerhof, Generalized gradient approximation made simple, Phys. Rev. Lett. 77 (18) (1996) 3865–3868. https://doi.org/10.1103/PhysRevLett.77.3865

[11] F. Zhou, M. Cococcioni, C.A. Marianetti, D. Morgan, G. Ceder, First-principles prediction of redox potentials in transition-metal compounds with LDA + U, Phys. Rev. B 70 (2004). article 235121. https://doi.org/10.1103/PhysRevB.70.235121

[12] M. Cococcioni, S. de Gironcoli, Linear response approach to the calculation of the effective interaction parameters in the LDA + U method, Phys. Rev. B 71 (2005). article 035105. https://doi.org/10.1103/PhysRevB.71.035105

[13] L. Wang, T. Maxisch, G. Ceder, Oxidation energies of transition metal oxides within the GGA + U framework, Phys. Rev. B 73 (2006). article 195107. https://doi.org/10.1103/PhysRevB.73.195107

[14] A. Jain, G. Hautier, S.P. Ong, C. Moore, C. Fischer, K.A. Persson, G. Ceder, Formation enthalpies by mixing GGA and GGA + U calculations, Phys. Rev. B 84 (4) (2011). article 045115. https://doi.org/10.1103/PhysRevB.84.045115

[15] S.L. Dudarev, G.A. Botton, S.Y. Savrasov, C.J. Humphreys, A.P. Sutton, Electron-energy-loss spectra and the structural stability of nickel oxide: An LSDA U study, Phys. Rev. B 57 (3) (1998). https://doi.org/10.1103/PhysRevB.57.1505

[16] M. Wang, A. Navrotsky, Enthalpy of formation of $LiNiO_2$, $LiCoO_2$ and their solid solution, $LiNi_{1-x}Co_xO_2$, Solid State Ionics 166 (1-2) (2004) 167–173. https://doi.org/10.1016/j.ssi.2003.11.004

[17] R. Schira, C. Latouche, DFT and hybrid-DFT calculations on the electronic properties of vanadate materials: theory meets experiments, New J. Chem. 44 (27) (2020) 11602–11607. https://doi.org/10.1039/D0NJ02316G

[18] A. Jain, S.P. Ong, G. Hautier, W. Chen, W.D. Richards, S. Dacek, S. Cholia, D. Gunter, D. Skinner, G. Ceder, K.A. Persson, Commentary: The Materials Project: A materials genome approach to accelerating materials innovation, APL Mater. 1 (1) (2013). https://doi.org/10.1063/1.4812323

[19] W.C. Mackrodt, A. Platonenko, R. Dovesi, Self-trapped excitons in diamond: A Δ-SCF approach, J. Chem. Phys. 157 (8) (2022). https://doi.org/10.1063/5.0097900

[20] M. Baskurt, P. Erhart, J. Wiktor, Direct, Indirect, and Self-Trapped Excitons in Cs2AgBiBr6, J. Phys. Chem. Lett. 15 (33) (2024). https://doi.org/10.1021/acs.jpclett.4c01604

[21] H.G. Hecht, The Interpretation of Diffuse Reflectance Spectra, J. Res. Natl. Bur. Stand.-A. Phys. Chem. 80A (4) (1976). https://doi.org/10.6028/jres.080A.056

[22] M. Sayer, Luminescence in the alkali metavandates, Phys. Status Solidi 269 (1) (1970) 269–277.

[23] T. Nakajima, M. Isobe, T. Tsuchiya, Y. Ueda, T. Kumagai, Direct fabrication of metavanadate phosphor films on organic substrates for white-light-emitting devices, Nat. Mater. 7 (2008) 735–740. https://doi.org/10.1038/nmat2244

[24] H. Gobrecht, G. Heinsohn, Über die Lumineszenz der Alkalivanadate, Zeitschrift für Physik 147 (1956) 350–360.

[25] S.L. Berdnikov, Y.M. Zelikin, Luminescence, excitation, and absorption spectra of alkali-metal metavanadate single crystals, Opt. Spectrosc. 54 (3) (1983) 273–277.

[26] G. Zatryb, M.M. Klak, On the choice of proper average lifetime formula for an ensemble of emitters showing non-single exponential photoluminescence decay, J. Phys. Condens. Matter 32 (2020). article 415902. https://doi.org/10.1088/1361-648X/ab9bcc

[27] H. Ronde, G. Blasse, The nature of the electronic transitions of the vanadate group, J. Inorg. Nucl. Chem. 40 (2) (1978) 215–219. https://doi.org/10.1016/0022-1902(78)80113-4

[28] T.D. Pham, N.A. Deskins, Efficient method for modeling polarons using electronic structure methods, J. Chem. Theory Comput. 16 (8) (2020) 5264–5278. https://doi.org/10.1021/acs.jctc.0c00374

[29] N.F. Mott, A.M. Stoneham, The lifetime of electrons, holes and excitons before self-trapping, J. Phys. C Solid State Phys. 10 (1977). article 3391. https://doi.org/10.1088/0022-3719/10/17/022

[30] S. Yuan, Z. Wang, M.L.F. Baron, K.H. Bevan, Ab initio insight into the formation of small polarons: A study across four metal peroxides, Phys. Rev. B 100 (2019). article 205201. https://doi.org/10.1103/PhysRevB.100.205201

[31] H. Jonsson, G. Mills, K.W. Jacobson, Nudged elastic band method for finding minimum energy paths of transitions, in: Classical and Quantum Dynamics in Condensed Phase Simulations, World Scientific, 1998, pp. 385–404. https://doi.org/10.1142/3816

[32] L. Zhang, C. Li, D. Jiang, K. Wang, G. Niu, L. Sui, K. Yuan, Y. Wang, Brightening self-trapped exciton emission in 2D metal-organic chalcogenolates via argentophilicity-mediated anisotropic compression, Nat. Commun. 16 (2025). article 7058. https://doi.org/10.1038/s41467-025-62170-6

[33] Y. Zhang, C. Zhang, X. Huang, Z. Yang, K.H.L. Zhang, Y. Yang, Barrierless self-trapping of photocarriers in Co_3O_4, J. Phys. Chem. Lett. 12 (50) (2021) 12033–12039. https://doi.org/10.1021/acs.jpclett.1c03716

[34] Z. Xing, Z. Zhou, G. Zhong, C.C.S. Chan, Y. Li, X. Zou, J.E. Halpert, H. Su, K.S. Wong, Barrierless exciton self-trapping and emission mechanism in low-dimensional copper halides, Adv. Funct. Mater. 32 (46) (2022). https://doi.org/10.1002/adfm.202207638

[35] A.M. de Paula, S. Li, B. Hou, S. Vadivel, D.C. Teles-Ferreira, A. Iudica, P. Kabacinski, H. Hosseini, J. McArthur, G. Cerullo, D.Y. Qiu, P. Guo, F.V.A. Camargo, Time-domain observation of ultrafast self-trapped exciton formation in lead-free double halide perovskites, J. Am. Chem. Soc. 147 (32) (2025) 28923–28931. https://doi.org/10.1021/jacs.5c06628

[36] Y. He, S. Liu, Z. Yao, Q. Zhao, P. Chabera, K. Zheng, B. Yang, T. Pullerits, J. Chen, Nature of self-trapped exciton emission in zero-dimensional Cs_2ZrCl_6 perovskite nanocrystals, J. Phys. Chem. Lett. 14 (34) (2023) 7665–7671. https://doi.org/10.1021/acs.jpclett.3c01878

[37] R. Singh, A. Singh, S. Kumar, S. Sapra, Ultrafast dynamics of self-trapped excitons in $Cs_2AgInCl_6:Al^{3+}$ double perovskite nanocrystals, Nano Lett. 24 (22) (2024) 6797–6804. https://doi.org/10.1021/acs.nanolett.4c01550

[38] K. Dave, W. Huang, T. Leśniewski, A. Lazarowska, D. Jankowski, S. Mahlik, R. Liu, Photoluminescence enhancement study in a Bi-doped $Cs_2AgInCl_6$ double perovskite by pressure and temperature-dependent self-trapped exciton emission, Dalton Trans. 51 (2022) 2026–2032. https://doi.org/10.1039/D1DT04047B

[39] Q. Sun, W.J. Yin, Thermodynamic stability trend of cubic perovskites, J. Am. Chem. Soc. 139 (42) (2017) 14905–14908. https://doi.org/10.1021/jacs.7b09379

[40] J.B. Varley, A. Janotti, C. Franchini, C.G. Van de Walle, Role of self-trapping in luminescence and p-type conductivity of wide-band-gap oxides, Phys. Rev. B 85 (2012). article 081109. https://doi.org/10.1103/PhysRevB.85.081109

[41] A.K.S. Song, R.T. Williams, Self-Trapped Excitons, Springer Berlin Heidelberg, 1993. https://doi.org/10.1007/978-3-642-85236-7

[42] B. Rana, M.P. Coons, J.M. Herbert, Detection and Correction of Delocalization Errors for Electron and Hole Polarons Using Density-Corrected DFT, J. Phys. Chem. Lett. 13 (23) (2022). https://doi.org/10.1021/acs.jpclett.2c01187

[43] A. Carta, I. Timrov, P. Mlkvik, A. Hampel, C. Ederer, Explicit demonstration of the equivalence between DFT + U and the Hartree-Fock limit of DFT + DMFT, Phys. Rev. Res. 7 (2025). article 013289. https://doi.org/10.1103/PhysRevResearch.7.013289

[44] J.K. Cooper, S.E. Reyes-Lillo, L.H. Hess, C.-M. Jiang, J.B. Neaton, I.D. Sharp, Physical origins of the transient absorption spectra and dynamics in thin-film semiconductors: the case of $BiVO_4$, J. Phys. Chem. C 122 (36) (2018) 20642–20652. https://doi.org/10.1021/acs.jpcc.8b06645

[45] J.S.P. Cresi, L.D. Mario, D. Catone, F. Martelli, A. Paladini, S. Turchini, S. D'Addato, P. Luches, P. O'Keeffe, Ultrafast formation of small polarons and the optical gap in CeO_2, J. Phys. Chem. Lett. 11 (14) (2020) 5686–5691. https://doi.org/10.1021/acs.jpclett.0c01590

[46] M. Schleuning, M. Kölbach, F.F. Abdi, K. Schwarzburg, M. Stolterfoht, R. Eichberger, R. van de Krol, D. Friedrich, H. Hempel, Generalized method to extract carrier diffusion length from photoconductivity transients: cases of $BiVO_4$, halide perovskites, and amorphous and crystalline silicon, PRX Energy 1 (2022). article 023008. https://doi.org/10.1103/PRXEnergy.1.023008

[47] D.C. Asebiah, A.N. Peters, L. Borgia, A. Nicolson, D.O. Scanlon, O.G. Reid, J.R. Neilson, $[(NH_3(CH_2)_7NH_3)]_2Sn_3I_{10}$, a vacancy-ordered three-dimensional tin(II) perovskite-derived semiconductor, Chem. Mater. 37 (5) (2025) 1983–1994. https://doi.org/10.1021/acs.chemmater.4c03411

[48] T. Wang, C. Caraiani, G.W. Burg, W. Chan, From two-dimensional electron gas to localized charge: Dynamics of polaron formation in organic semiconductors, Phys. Rev. B 91 (2015). article 041201. https://doi.org/10.1103/PhysRevB.91.041201

[49] A.R. Elmaslmane, M.B. Watkins, K.P. McKenna, First-principles modeling of polaron formation in TiO_2 polymorphs, J. Chem. Theory Comput. 14 (7) (2018) 3740–3751. https://doi.org/10.1021/acs.jctc.8b00199

[50] K. Momma, F. Izumi, VESTA 3 for three-dimensional visualization of crystal, volumetric and morphology data, J. Appl. Crystallogr. 44 (6) (2011) 1272–1276. https://doi.org/10.1107/S0021889811038970